Transition strengths in odd-odd ^{86}Nb

M. Wiedeking,[1,2] R. A. Kaye,[1,*] G. Z. Solomon,[1] S. L. Tabor,[1] J. Döring,[3,†] G. D. Johns,[4] F. Cristancho,[5] M. Devlin,[6] F. Lerma,[6] D. G. Sarantites,[6] I. Y. Lee,[7] and A. O. Macchiavelli[7]

[1]*Department of Physics, Florida State University, Tallahassee, Florida 32306*

[2]*Department of Physics, University of Surrey, Guildford, Surrey GU2 5XH, United Kingdom*

[3]*Department of Physics, University of Notre Dame, Notre Dame, Indiana 46556*

[4]*Los Alamos National Laboratory, Los Alamos, New Mexico 87545*

[5]*Departamento de Física, Universidad Nacional de Colombia, Bogotá, Colombia*

[6]*Chemistry Department, Washington University, St. Louis, Missouri 63130*

[7]*Nuclear Science Division, Lawrence Berkeley National Laboratory, Berkeley, California 94720*

(Received 20 January 2000; published 20 July 2000)

High angular momentum states in odd-odd ^{86}Nb were populated through the ^{58}Ni(^{32}S,3pn) reaction at 135 MeV. Recoiling ^{86}Nb nuclei were stopped in a thick Ta backing. Prompt multi-γ coincidences with evaporated charged particles were detected using the full array of Gammasphere and the Microball. Mean lifetimes of 51 levels in ^{86}Nb were measured using the Doppler-shift attenuation method. Strongly alternating magnetic dipole transition strengths were observed in the yrast positive-parity bands. Most of the transition quadrupole moments inferred from the lifetimes lie in the range of 1 to 2.7 e b, which would correspond to quadrupole deformations β_2 of 0.10 to 0.27 in a rotational model. Comparison with Hartree-Fock-Bogoliubov cranking calculations suggests triaxial to oblate shapes.

PACS number(s): 23.20.En, 23.20.Lv, 21.10.Re, 27.50.+e

I. INTRODUCTION

The shapes of nuclei in the f-p-g shell often vary rapidly with Z,N, rotation, the number of quasiparticles, and the orbitals occupied by the quasiparticles. In view of this variability, it is rather surprising that some aspects of the structure of odd-odd nuclei remain so constant across the shell [1]. Although it is not unexpected that the $\pi g_{9/2} \otimes \nu g_{9/2}$ band would remain yrast across the shell, since the unique parity $g_{9/2}$ orbital carries the highest angular momentum, it is surprising that other characteristics of this band would vary so little. In particular, the energies of levels in the $\pi g_{9/2} \otimes \nu g_{9/2}$ bands exhibit a large signature splitting which always reverses phase around the 9^+ state. A large alternation also occurs in the strengths of the $M1$ transitions between the signatures, but there is no sign of the phase reversal seen in the energy splittings. These characteristics continue to appear in new investigations [2–6].

Although most studies of $\pi g_{9/2} \otimes \nu g_{9/2}$ bands have involved well-deformed nuclei near the middle of the f-p-g shell, recent investigations of the odd-odd transitional nucleus ^{86}Nb have revealed a similar band structure in spite of an apparently limited deformation. Possible band structures in ^{86}Nb were first identified in an experiment at Daresbury Laboratory [7]. The level scheme was greatly expanded with data from the early implementation of Gammasphere in conjunction with the Microball [8]. The level scheme of ^{86}Nb based on this and later work is given in Fig. 1. Bands 3 and 4 in this figure are the yrast $\pi g_{9/2} \otimes \nu g_{9/2}$ band pair whose characteristics are discussed in Ref. [8]. The negative-parity band structure has been rearranged somewhat, based on the results of the present work.

Mean lifetimes of 360(100) and 1210(200) ps were measured for the 6^- and 8^+ states at Laboratorio TANDAR using the recoil-distance method [9]. These values imply quite reasonable transition strengths of $B(E1) = 1.2 \times 10^{-5}$ Weisskopf units (W.u.) and $B(E2) = 11$ W.u. for the 494.2 and 274.5 keV decays.

To resolve some remaining uncertainties, the parities of the 26.4, 274.5, and 494.2 keV states were determined directly by measuring the linear polarizations of the connecting γ transitions in an experiment using a four-crystal ''Clover'' detector at the FSU Superconducting Accelerator Laboratory [10]. The results are included in Fig. 1. In conjunction with the earlier lifetime measurement [9], they show that the 248.1 keV decay has a surprisingly weak $B(M1)$ transition strength of 1.4×10^{-3} W.u.

The wide difference in collectivity between the 248.1 and 274.5 keV transitions in bands 3 and 4 leads to more questions about the deformation and degree of collectivity in ^{86}Nb. Although the energy spacings in bands 3 and 4 follow the characteristic patterns seen in more deformed nuclei, the apparent mixing with band 2 is unanticipated. Questions also arise about the degree and variation of collectivity in many of the other bands. The energy spacings in bands 2 and 5 do not increase regularly at lower spins. Both bands 2 and 9 (in the labeling of Ref. [8]) become yrast at higher spins. Are they more deformed? Do the states at 5027.3 and 5533.1 keV represent less collective, aligned configurations? The present experiment was undertaken to answer some of these questions by measuring the lifetimes of many states in ^{86}Nb using the Doppler-shift attenuation method (DSAM).

*Present address: Department of Physics and Chemistry, Purdue University Calumet, Hammond, Indiana 46323.

†Present address: GSI, D-64291 Darmstadt, Germany.

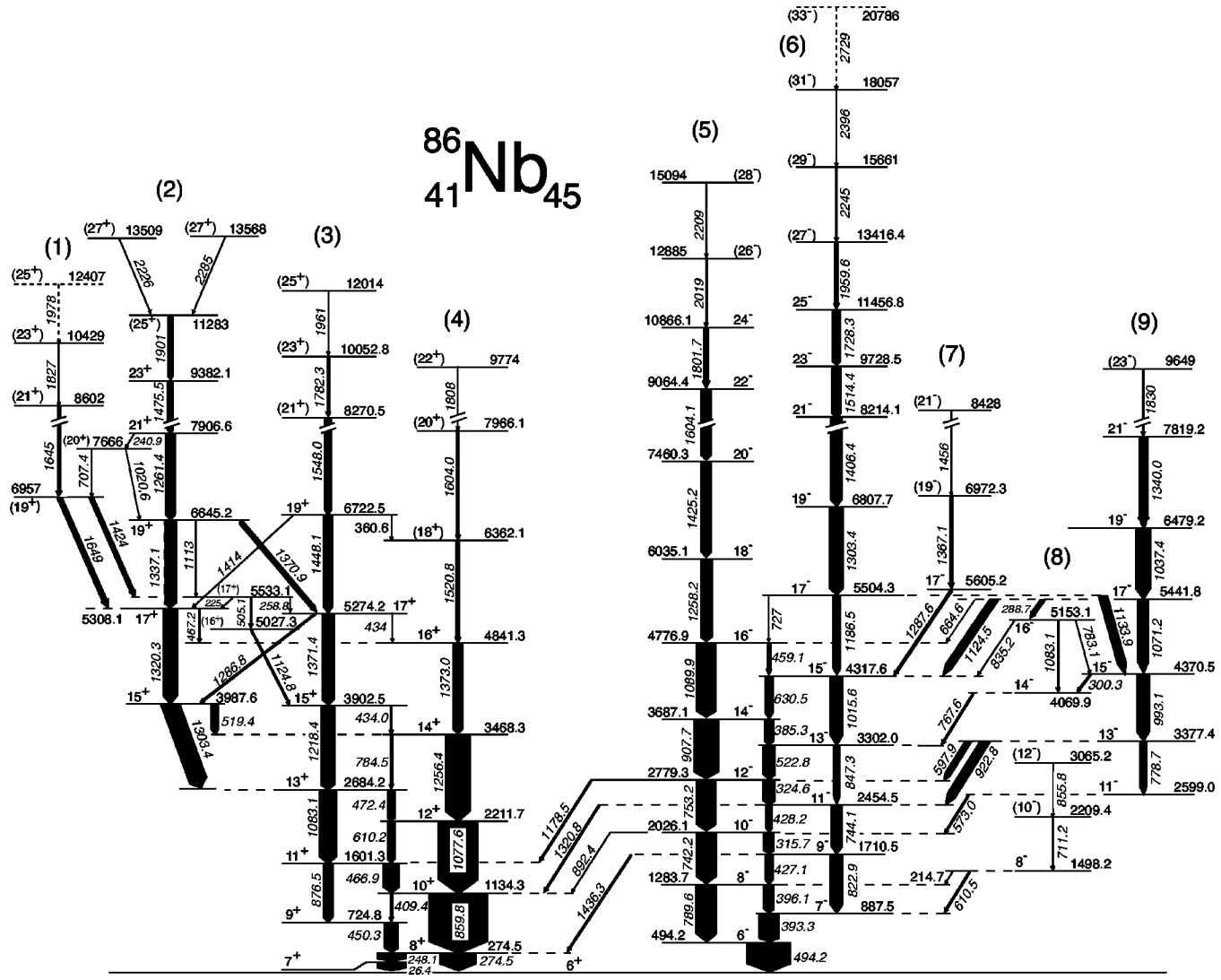

FIG. 1. The level scheme of ^{86}Nb as deduced from Refs. [8,10]. The vertical scale is reduced by a factor of 2 above an excitation energy of 8000 keV. The arbitrary numbers above the decay sequences are intended only to facilitate the discussion. Bands 6 and 9 have been rearranged, as discussed in the text.

II. EXPERIMENTAL PROCEDURE

With beams from the 88-Inch Cyclotron at Lawrence Berkeley National Laboratory, high spin states in ^{86}Nb were populated using the fusion-evaporation reaction ^{58}Ni(^{32}S,3pn) at 135 MeV and a beam intensity of 3.5 particle nA. The recoil velocity of the reaction products was $v/c \approx 0.035$. The experiment, optimized for lifetime measurements using the Doppler-shift attenuation method, made use of a 415 μg/cm^2 thick ^{58}Ni target which was evaporated on a 10.3 mg/cm^2 Ta backing used as the stopping material for the recoiling nuclei.

Gamma rays from the reaction were detected with the Gammasphere [11] array. The evaporated charged particles were detected and identified with the Microball [12]. This array consists of 95 CsI(Tl) scintillators covering 97% of the full sphere around the target. The Microball has a proton detection efficiency of 84%.

The collected data were sorted into different 3000$\times$3000 channel square matrices. To obtain optimum selection of ^{86}Nb events, all matrices were gated on the requirement of two or three protons detected in the Microball. Then, to remove contamination from the very strong ^{86}Zr channel, 2.1 times the corresponding 4p gated matrices were subtracted. The matrices were also gated on the requirement of a third coincident γ ray. To select the positive-parity bands this third γ ray was required to be one of the following lines: 248.1, 274.5, 450.3, 466.9, 472.4, 859.8, 1077.6, or 1083.1 keV. Separate matrices were sorted to enhance the negative-parity bands by requiring either the 315.7, 324.6, 393.3, 396.1, 427.1, 428.2, 494.2, 742.2, 744.1, 789.6, 822.9, 847.3, or 993.1 keV lines as the third coincident γ ray.

γ rays from any of the detectors were sorted onto one axis of the square arrays to allow for a second γ gate in selecting the line shapes. Only lines from detectors at approximately the same θ angle were sorted onto the second axis, from which the line shapes to be fitted were obtained. The following pairs of detector rings were combined: 31.72° with 37.38°, 50.07° with 58.28°, 121.72° with 129.93°, and

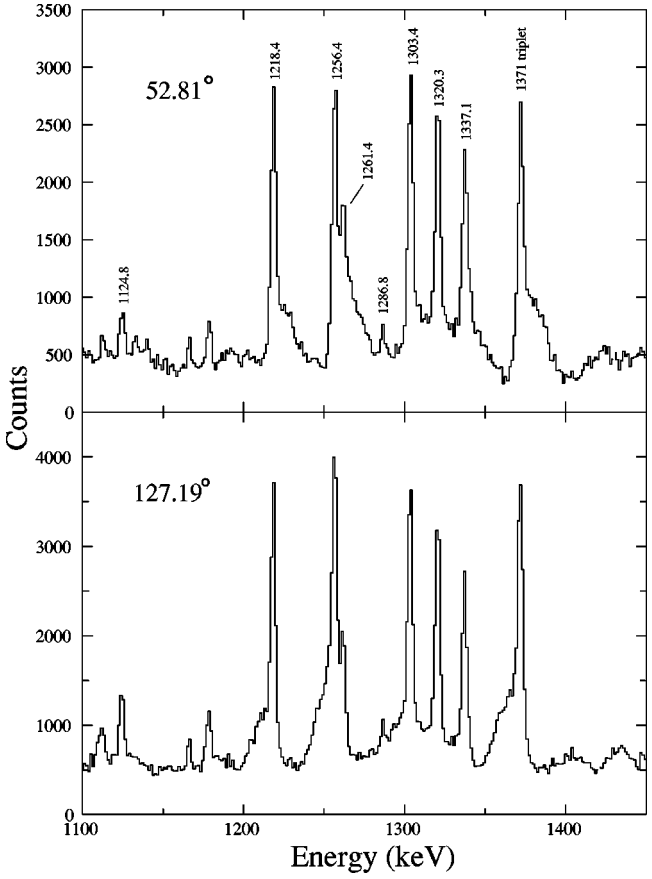

FIG. 2. A comparison of forward (52.81°) and backward (127.19°) angle spectra generated by adding $\pi = +$ low-spin gates.

142.62° with 148.28°. These combinations yield weighted average angles of 34.55° (eight active detectors), 52.81° (15 active detectors), 127.19° (15 active detectors), and 145.45° (ten active detectors), respectively.

With these sorted data it was possible to create spectra by adding up many gates set on low-lying ^{86}Nb transitions. These projected spectra provided line shapes for the determination of lifetimes. Examples of the spectra at forward and backward angles for the same region are shown in Fig. 2.

III. LIFETIME MEASUREMENTS

Mean lifetimes for the shorter-lived higher-lying states in all bands (1 to 9) were analyzed by applying the Doppler-shift attenuation method to the experimental line shapes. The DSAM compares the decay time of the recoiling nuclei with their slowing-down time in the target and backing material. This comparison was carried out using the computer simulation code FITS [13] which integrates over the thickness of the target and determines the distribution of recoil velocities as the nuclei slow down and decay. In addition the program corrects for feeding from both known and unknown higher-lying states as well as for finite detector solid angle and resolution and for the energy dependence of the reaction cross sections as the beam decelerates through the target.

The theoretical line shapes generated by FITS for a range of possible mean lifetimes were compared to the coincidence

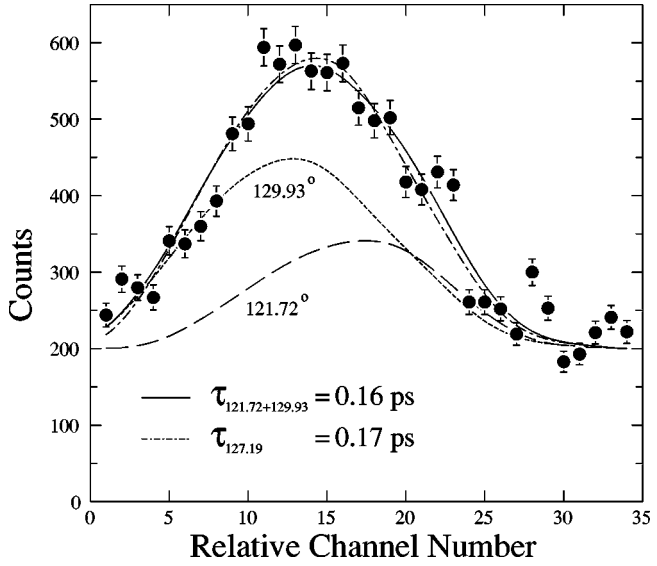

FIG. 3. Comparison between the sum of the theoretical line-shapes calculated at 121.72° and 129.93° and the theoretical line shape calculated at 127.19°. Unless otherwise noted, the dispersion is 1.33 keV/channel on the line shape graphs.

spectra at each of the four angles, 34.55°, 52.81°, 127.19°, and 145.45°. The lifetimes giving the best fit (lowest χ^2) were first determined separately for each angle of observation. The uncertainty of individual lifetimes was determined by finding the lifetime value above and below the best fit value at which χ^2 increases by one unit. The individual lifetimes were averaged to determine the accepted values. The uncertainties listed for the accepted lifetimes are based on both the standard deviation of the averaged lifetimes and the uncertainties in the individual lifetime fits.

As mentioned earlier, the data from pairs of nearby detector rings were combined to improve the statistics. These data were fitted using the average angle, weighted by the number of active detectors in each ring. This approximation was tested in several cases by adding (with proper scaling) theoretical line shapes calculated separately at each ring angle and comparing this to the theoretical line shapes calculated for the average angle. Figure 3 shows an example of such a comparison for the detector rings at 121.72° and 129.93° where the differences in $\cos\theta$ are greatest. The small differences between the two approaches are well within the statistical uncertainties in the data.

Each line shape was first fitted with no feeding correction to determine the effective lifetime, which represents an upper limit for the lifetime of the state. Each transition, except for the highest one in each cascade with adequate statistics for fitting, was fitted again, taking direct (known) feeding and side (unknown) feeding into account. The direct feeding correction used the effective lifetime of the state or states immediately above, and the lifetimes were varied until the best fit was obtained. Figure 4 shows the impact of taking known and unknown feeding into account for the 1089.9 and 1303.4 keV line shapes. Due to the inability to correct for the feeding of the state above, only upper-limit effective lifetimes were determined for the highest fitted state in each band.

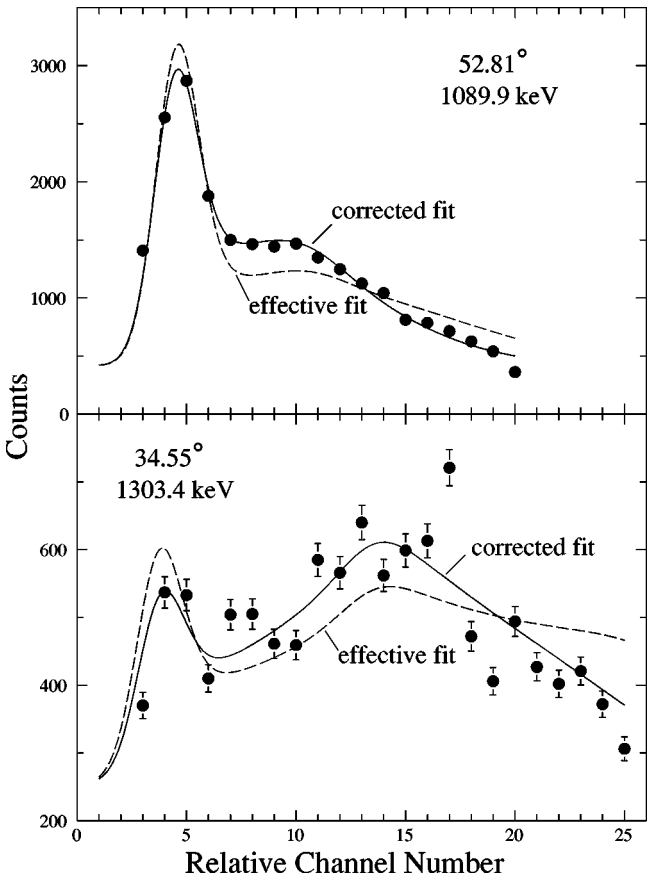

FIG. 4. A comparison of the best fits with (solid line) and without (dashed line) correction for direct and side feeding. Both line shapes are from negative-parity bands.

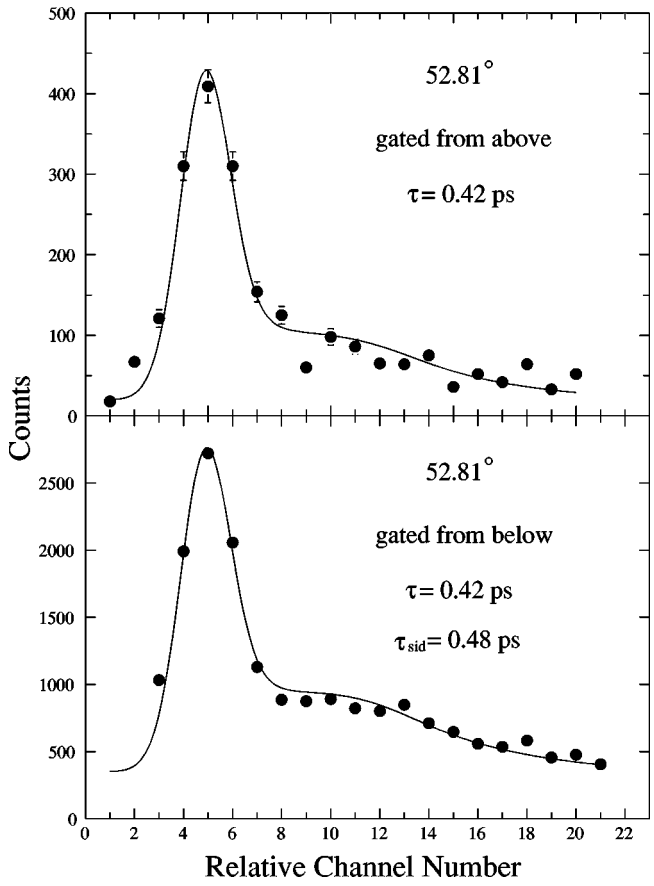

FIG. 5. The comparison of the 1218.4 keV transition at 127.19° gated from above (GFA) and below (GFB).

For a number of transitions in the positive-parity bands, side-feeding times were determined by fitting line shapes obtained by gating from above (GFA) the transition of interest to eliminate the contribution of side feeding. These lifetimes, determined separately at each angle, were then held fixed in fitting the same line shapes gated from below (GFB). Only the side-feeding lifetimes were allowed to vary until the best fits were obtained. An example of GFA and GFB line shapes is given in Fig. 5 in the case of the 1218.4 keV transition. Extracting reliable side-feeding times from the negative-parity bands was not successful since the fits were not sensitive enough to feeding corrections from unknown states due to smaller side-feeding intensities.

The side-feeding times determined were then compared with the effective lifetimes of the states immediately above. Although there is some variation, due mainly to statistical variations, the side-feeding times averaged about 35% of the effective lifetime above. This average was adopted for all the final fits. The side-feeding intensity was determined from the balance of feeding and decay intensities taken from Ref. [8].

IV. RESULTS

Line shapes were extracted from as many transitions and angles as possible to measure the lifetimes with the DSAM. All lifetimes measured in the present work are listed in Table I. The effective lifetimes are the average of values obtained at the various angles at which lifetimes could be measured. Corrected lifetimes are listed for each angle along with the accepted lifetime which is taken as the average of the individual lifetimes. In a few cases, it was not possible to obtain reliable line shapes at a particular angle. These are left as blanks in Table I.

The line shapes of the 1514.4 keV transition in band 6 are shown at all four average angles in Fig. 6 as an example of the variation with angle. Figure 7 illustrates the variation of the line shapes from a shortest to one of the longest lifetimes measured.

In most cases it was possible to fit each transition individually, without interference from other peaks, by a judicious choice of gates. Where this was not possible, a modified version of FITS was used to fit two overlapping line shapes simultaneously, by comparison with the properly scaled sum of the two theoretical line shapes. Figure 8 shows an example for the 1083.1 and 1077.6 keV lines in bands 3 and 4, respectively. This method proved very reliable as can be seen from states where lifetimes were measured separately from both individual lines and from simultaneous fits of overlapping pairs of lines, e.g., the transition pairs 519.4–1303.4 and 1371.4–1286.8 keV in Table I.

A. Positive-parity states

In order to get the best statistical results, all low-spin ($<15\hbar$) gates in coincidence and below the transition of

TABLE I. Energies, effective lifetimes, mean lifetimes at each angle, and the accepted lifetimes in ^{86}Nb. The effective and accepted lifetimes are the average of all possible angles. Energies and spin assignments were taken from Ref. [8].

E_x	I_i^π	I_f^π	E_γ	τ_{eff} [a]	τ (ps)				τ_{acc}
(keV)			(keV)	(ps)	34.55°	52.81°	127.19°	145.45°	(ps)
					Band 1				
10429	(23^+)	(21^+)	1827	$0.11^{+0.07}_{-0.06}$					
8602	(21^+)	(19^+)	1645	$0.53^{+0.22}_{-0.19}$	$0.26^{+0.22}_{-0.18}$		$0.52^{+0.25}_{-0.23}$	$0.53^{+0.22}_{-0.16}$	$0.44^{+0.22}_{-0.16}$
6957	(19^+)	(17^+)	1424	$1.01^{+0.48}_{-0.43}$	$0.44^{+0.09}_{-0.08}$	$0.64^{+0.13}_{-0.14}$	$1.05^{+0.50}_{-0.30}$	$0.76^{+0.80}_{-0.38}$	$0.72^{+0.35}_{-0.26}$
					Band 2				
13568	(27^+)	(25^+)	2285	$0.09^{+0.06}_{-0.04}$					
13509	(27^+)	(25^+)	2226	$0.09^{+0.04}_{-0.03}$					
11283	(25^+)	23^+	1901	$0.19^{+0.06}_{-0.05}$	$0.05^{+0.04}_{-0.02}$	$0.10^{+0.07}_{-0.05}$	$0.09^{+0.05}_{-0.05}$	$0.16^{+0.08}_{-0.05}$	$0.10^{+0.06}_{-0.04}$
9382	23^+	21^+	1476	$0.46^{+0.10}_{-0.08}$	$0.38^{+0.13}_{-0.12}$	$0.40^{+0.12}_{-0.11}$	$0.22^{+0.17}_{-0.19}$	$0.29^{+0.08}_{-0.09}$	$0.32^{+0.08}_{-0.08}$
7907	21^+	19^+	1261	$1.04^{+0.26}_{-0.24}$	$0.64^{+0.13}_{-0.11}$	$0.60^{+0.14}_{-0.11}$	$0.64^{+0.13}_{-0.10}$	$0.72^{+0.18}_{-0.14}$	$0.65^{+0.22}_{-0.20}$
6645	19^+	17^+	1337	$1.60^{+0.30}_{-0.27}$	$0.76^{+0.28}_{-0.17}$	$0.74^{+0.10}_{-0.09}$	$0.82^{+0.08}_{-0.07}$	$0.87^{+0.46}_{-0.25}$	$0.80^{+0.23}_{-0.21}$
5308	17^+	15^+	1320	$1.66^{+0.23}_{-0.20}$	$0.66^{+0.09}_{-0.09}$	$0.64^{+0.09}_{-0.07}$	$0.58^{+0.07}_{-0.06}$	$0.40^{+0.05}_{-0.06}$	$0.57^{+0.14}_{-0.13}$
3988	15^+	14^+	519	$1.76^{+0.24}_{-0.21}$ [c]	$0.31^{+0.26}_{-0.17}$	$0.28^{+0.14}_{-0.10}$		$0.32^{+0.22}_{-0.20}$	$0.31^{+0.11}_{-0.09}$ [c]
		13^+	1303	$1.76^{+0.24}_{-0.21}$ [c]		$0.38^{+0.05}_{-0.06}$	$0.32^{+0.05}_{-0.09}$	$0.26^{+0.10}_{-0.07}$	$0.31^{+0.11}_{-0.09}$ [c]
					Band 3				
12014	(25^+)	(23^+)	1961	$0.06^{+0.04}_{-0.03}$					
10053	(23^+)	(21^+)	1782	$0.26^{+0.12}_{-0.10}$		$0.04^{+0.09}_{-0.04}$	$0.22^{+0.10}_{-0.09}$	$0.22^{+0.13}_{-0.07}$	$0.16^{+0.10}_{-0.09}$
8271	(21^+)	19^+	1548	$0.40^{+0.09}_{-0.08}$	$0.18^{+0.13}_{-0.07}$	$0.12^{+0.10}_{-0.09}$	$0.15^{+0.11}_{-0.07}$	$0.26^{+0.16}_{-0.14}$	$0.18^{+0.10}_{-0.07}$
6723	19^+	17^+	1448	$0.67^{+0.15}_{-0.13}$	$0.42^{+0.10}_{-0.10}$	$0.12^{+0.15}_{-0.07}$	$0.16^{+0.08}_{-0.06}$	$0.36^{+0.29}_{-0.23}$	$0.27^{+0.16}_{-0.13}$
5274	17^+	15^+	1287	$1.15^{+0.16}_{-0.13}$ [c]	$0.42^{+0.34}_{-0.25}$	$0.52^{+0.34}_{-0.22}$	$0.30^{+0.18}_{-0.13}$	$0.61^{+0.38}_{-0.22}$	$0.44^{+0.11}_{-0.09}$ [c]
		15^+	1371	$1.15^{+0.16}_{-0.13}$ [c]	$0.46^{+0.11}_{-0.08}$	$0.50^{+0.09}_{-0.07}$	$0.30^{+0.06}_{-0.04}$	$0.38^{+0.07}_{-0.08}$	$0.44^{+0.11}_{-0.09}$ [c]
3903	15^+	13^+	1218	$1.67^{+0.15}_{-0.13}$	$0.47^{+0.09}_{-0.08}$	$0.46^{+0.06}_{-0.05}$	$0.56^{+0.07}_{-0.06}$	$0.48^{+0.08}_{-0.06}$	$0.49^{+0.08}_{-0.06}$
2684	13^+	11^+	1083	$2.60^{+0.56}_{-0.49}$	$0.41^{+0.14}_{-0.11}$	$0.49^{+0.11}_{-0.09}$		$0.64^{+0.40}_{-0.22}$	$0.51^{+0.14}_{-0.11}$
1601	11^+	9^+	877	$3.39^{+0.67}_{-0.58}$	$0.47^{+0.23}_{-0.16}$	$0.53^{+0.18}_{-0.14}$	$0.53^{+0.18}_{-0.13}$	$0.42^{+0.20}_{-0.15}$	$0.49^{+0.15}_{-0.12}$
					Band 4				
6362	(18^+)	16^+	1521	$0.43^{+0.17}_{-0.15}$					
4841	16^+	14^+	1373	$1.73^{+0.38}_{-0.34}$	$0.94^{+0.30}_{-0.23}$	$0.56^{+0.24}_{-0.19}$			$0.75^{+0.27}_{-0.24}$
3468	14^+	12^+	1256	$1.82^{+0.35}_{-0.30}$	$0.46^{+0.13}_{-0.10}$	$0.33^{+0.10}_{-0.07}$	$0.62^{+0.14}_{-0.11}$	$0.57^{+0.19}_{-0.13}$	$0.50^{+0.14}_{-0.11}$
2212	12^+	10^+	1078	$2.68^{+0.56}_{-0.52}$			$0.72^{+0.12}_{-0.09}$	$0.62^{+0.15}_{-0.10}$	$0.67^{+0.11}_{-0.09}$
275	8^+	6^+	275						1210(200) [b]
					Band 5				
12885	(26^-)	24^-	2019	$0.03^{+0.03}_{-0.02}$					
10866	24^-	22^-	1802	$0.08^{+0.04}_{-0.03}$	$0.05^{+0.08}_{-0.04}$	$0.06^{+0.03}_{-0.03}$	$0.06^{+0.04}_{-0.03}$	$0.08^{+0.04}_{-0.04}$	$0.06^{+0.03}_{-0.02}$
9064	22^-	20^-	1604	$0.15^{+0.06}_{-0.05}$	$0.05^{+0.04}_{-0.04}$	$0.06^{+0.02}_{-0.02}$	$0.10^{+0.03}_{-0.02}$	$0.10^{+0.02}_{-0.03}$	$0.08^{+0.02}_{-0.02}$
7460	20^-	18^-	1425	$0.34^{+0.09}_{-0.07}$	$0.15^{+0.07}_{-0.05}$	$0.13^{+0.06}_{-0.05}$	$0.26^{+0.07}_{-0.07}$	$0.21^{+0.07}_{-0.05}$	$0.19^{+0.07}_{-0.05}$

TABLE I. (*Continued*).

E_x (keV)	I_i^π	I_f^π	E_γ (keV)	τ_{eff} [a] (ps)	τ (ps) 34.55°	52.81°	127.19°	145.45°	τ_{acc} (ps)
6035	18^-	16^-	1258	$0.51^{+0.06}_{-0.05}$	$0.18^{+0.06}_{-0.04}$	$0.18^{+0.04}_{-0.04}$	$0.19^{+0.05}_{-0.04}$	$0.21^{+0.04}_{-0.04}$	$0.19^{+0.04}_{-0.03}$
4777	16^-	15^-	459	$1.20^{+0.13}_{-0.11}$ [c]			$0.41^{+0.06}_{-0.05}$	$0.48^{+0.09}_{-0.10}$	$0.49^{+0.08}_{-0.06}$ [c]
		14^-	1090	$1.20^{+0.13}_{-0.11}$ [c]	$0.58^{+0.08}_{-0.05}$	$0.49^{+0.03}_{-0.04}$			$0.49^{+0.08}_{-0.06}$ [c]
3687	14^-	12^-	908	$3.06^{+0.66}_{-0.53}$	$1.10^{+0.17}_{-0.13}$	$0.90^{+0.07}_{-0.07}$	$1.22^{+0.16}_{-0.12}$	$1.13^{+0.13}_{-0.11}$	$1.09^{+0.16}_{-0.13}$
494	6^-	6^+	494						360(100)[b]
				Band 6					
13416	(27^-)	25^-	1960	$0.06^{+0.02}_{-0.02}$					
11457	25^-	23^-	1728	$0.18^{+0.04}_{-0.03}$	$0.12^{+0.07}_{-0.05}$	$0.09^{+0.06}_{-0.04}$	$0.16^{+0.08}_{-0.06}$	$0.10^{+0.03}_{-0.02}$	$0.12^{+0.04}_{-0.03}$
9729	23^-	21^-	1514	$0.25^{+0.05}_{-0.04}$	$0.07^{+0.04}_{-0.03}$	$0.07^{+0.03}_{-0.03}$	$0.08^{+0.03}_{-0.03}$	$0.08^{+0.04}_{-0.03}$	$0.08^{+0.03}_{-0.02}$
8214	21^-	19^-	1406	$0.38^{+0.05}_{-0.04}$	$0.16^{+0.06}_{-0.05}$	$0.22^{+0.05}_{-0.04}$	$0.18^{+0.04}_{-0.03}$	$0.16^{+0.04}_{-0.04}$	$0.18^{+0.04}_{-0.03}$
6808	19^-	17^-	1303	$0.57^{+0.07}_{-0.05}$	$0.27^{+0.05}_{-0.04}$	$0.30^{+0.04}_{-0.04}$	$0.21^{+0.05}_{-0.05}$	$0.22^{+0.03}_{-0.04}$	$0.25^{+0.05}_{-0.04}$
5504	17^-	15^-	1134	$1.06^{+0.19}_{-0.16}$ [c]	$0.53^{+0.10}_{-0.09}$	$0.35^{+0.07}_{-0.06}$	$0.45^{+0.11}_{-0.10}$	$0.39^{+0.05}_{-0.04}$	$0.46^{+0.11}_{-0.09}$ [c]
		15^-	1187	$1.06^{+0.19}_{-0.16}$ [c]	$0.45^{+0.10}_{-0.08}$	$0.52^{+0.08}_{-0.07}$	$0.68^{+0.20}_{-0.15}$	$0.34^{+0.06}_{-0.06}$	$0.46^{+0.11}_{-0.09}$ [c]
4318	15^-	13^-	1016	$2.31^{+0.29}_{-0.26}$	$0.98^{+0.25}_{-0.18}$	$0.58^{+0.08}_{-0.07}$	$0.58^{+0.09}_{-0.06}$	$0.64^{+0.11}_{-0.08}$	$0.69^{+0.16}_{-0.13}$
3302	13^-	12^-	523	$3.79^{+0.48}_{-0.41}$	$0.61^{+0.18}_{-0.13}$	$0.78^{+0.10}_{-0.09}$	$0.56^{+0.07}_{-0.06}$	$0.66^{+0.10}_{-0.09}$	$0.65^{+0.10}_{-0.09}$
				Band 7					
8428	(21^-)	(19^-)	1456	$0.23^{+0.09}_{-0.07}$					
6972	(19^-)	17^-	1367	$0.44^{+0.13}_{-0.10}$	$0.43^{+0.13}_{-0.12}$	$0.35^{+0.09}_{-0.08}$	$0.29^{+0.12}_{-0.12}$	$0.36^{+0.08}_{-0.08}$	$0.36^{+0.08}_{-0.07}$
5605	17^-	15^-	1288	$0.69^{+0.31}_{-0.23}$		$0.17^{+0.21}_{-0.17}$	$0.24^{+0.19}_{-0.16}$		$0.21^{+0.18}_{-0.16}$
				Band 8					
5153	16^-	15^-	835	$1.47^{+0.69}_{-0.50}$	$0.15^{+0.20}_{-0.13}$	$0.07^{+0.18}_{-0.06}$	$0.36^{+0.39}_{-0.30}$	$0.60^{+0.55}_{-0.45}$	$0.30^{+0.27}_{-0.21}$
4070	14^-	13^-	768	$2.79^{+1.30}_{-1.05}$	$0.56^{+0.58}_{-0.33}$	$0.53^{+0.40}_{-0.22}$	$1.16^{+0.72}_{-0.41}$	$0.35^{+0.44}_{-0.30}$	$0.65^{+0.38}_{-0.31}$
				Band 9					
9649	(23^-)	21^-	1830	$0.33^{+0.11}_{-0.09}$					
7819	21^-	19^-	1340	$1.30^{+0.31}_{-0.25}$	$1.14^{+0.25}_{-0.17}$	$1.33^{+0.21}_{-0.18}$	$1.06^{+0.11}_{-0.09}$	$1.04^{+0.12}_{-0.09}$	$1.14^{+0.27}_{-0.23}$
6479	19^-	17^-	1037	$3.71^{+0.47}_{-0.41}$	$1.56^{+0.33}_{-0.18}$	$1.42^{+0.18}_{-0.15}$	$2.26^{+0.40}_{-0.31}$	$1.98^{+0.42}_{-0.29}$	$1.81^{+0.39}_{-0.30}$
5442	17^-	15^-	1071	$1.95^{+0.57}_{-0.48}$ [c]	$0.15^{+0.24}_{-0.15}$		$0.29^{+0.19}_{-0.15}$	$0.13^{+0.23}_{-0.13}$	$0.21^{+0.12}_{-0.09}$ [c]
		15^-	1125	$1.95^{+0.57}_{-0.48}$ [c]			$0.27^{+0.09}_{-0.07}$	$0.19^{+0.45}_{-0.16}$	$0.21^{+0.12}_{-0.09}$ [c]
4371	15^-	13^-	993	$2.86^{+0.37}_{-0.29}$	$0.90^{+0.25}_{-0.25}$	$0.78^{+0.14}_{-0.10}$	$0.96^{+0.18}_{-0.14}$	$0.94^{+0.20}_{-0.14}$	$0.90^{+0.13}_{-0.11}$
3377	13^-	11^-	779	$3.86^{+1.45}_{-1.30}$ [c]	$0.44^{+0.39}_{-0.28}$	$0.46^{+0.23}_{-0.19}$	$1.68^{+1.35}_{-0.60}$	$1.42^{+1.88}_{-0.62}$	$0.94^{+0.48}_{-0.42}$ [c]
		11^-	923	$3.86^{+1.45}_{-1.30}$ [c]	$0.96^{+0.56}_{-0.30}$	$0.98^{+0.38}_{-0.24}$		$0.62^{+0.21}_{-0.15}$	$0.94^{+0.48}_{-0.39}$ [c]

[a] Average of effective lifetimes measured at all possible angles.

[b] Mean lifetime taken from Ref. [9].

[c] τ_{eff} and τ_{acc} are determined by averaging all available values for both transitions.

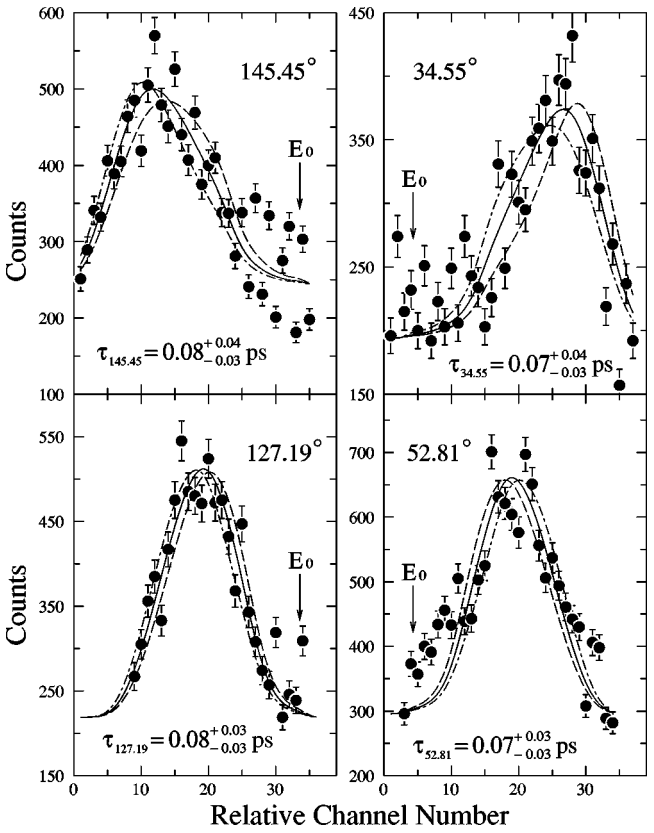

FIG. 6. The 1514.4 keV transition in band 6 fitted individually at all four angles. Fits representing the uncertainty limits are shown with dashed and dashed-dotted lines. The expected position of an unshifted 1514.4 keV line is indicated with an arrow.

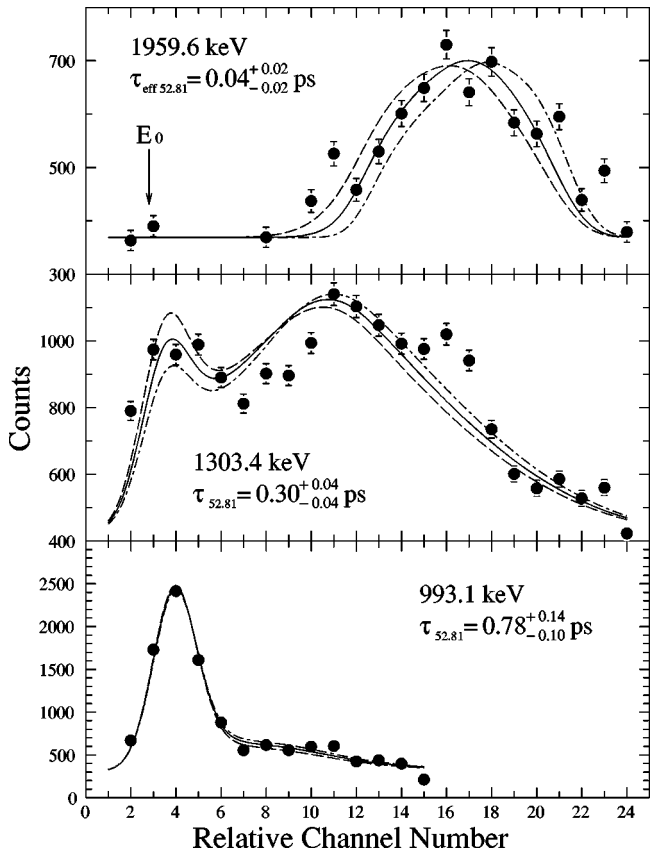

FIG. 7. Typical fits at 52.81° taken from bands 6 and 9. Top: 1959.6 keV, one of the shortest-lived states measured in this work (band 6). Middle: the 1303.4 keV from a medium-lived state (band 6). Bottom: the 993.1 keV transition from a long-lived state (band 9). The dipersion for the 1959.6 keV graph is 2.67 keV/channel.

interest were generally added together. In some cases however, this procedure was not possible due to interference or contamination and fewer, more selective, gates were chosen.

The highest-lying states in bands 1, 2, 3, and 4 for which line shapes could be extracted and lifetimes determined were the 1827 keV (23^+), 2226 and 2285 keV (27^+), 1961 keV (25^+), and 1520.8 keV (18^+) transitions (levels), respectively; thus only effective lifetimes are quoted for these states. The line shapes which were not separable from other ones and had to be fitted in pairs using the modified version of FITS were 1337.1 (backward angles only), 1320.3, 1303.4 (backward angles only), 1548.0 (forward angles only), 1448.1 (forward angles only), 1371.4 (all angles), 1520.8 (all angles), 1373.0 (forward angles only), and 1077.6 keV (backward angles only).

In most rotational bands, the lifetimes of states decrease steadily with increasing spins and transition energies. This reduces the effects of feeding corrections and improves the accuracy of the DSAM technique. However, this is not the case in the lower part of band 2, where already the nearly equal γ-ray energies indicate a deviation from normal behavior. An examination of Fig. 2 shows rather similar line shapes for all those decays. More quantitatively, the effective lifetimes of the 15^+,17^+, and 19^+ states, shown in Table I, are nearly equal, and the corrected lifetimes of the 15^+ and 17^+ levels are actually shorter than that of the 19^+ one. This ''shadowing'' by the longer lived 19^+ states increases the uncertainties in the lifetimes of the 15^+ and 17^+ states in band 2. However, there is no doubt that their lifetimes are shorter than that of the 19^+ state, and the lifetime measurements made using the 519.4 keV transition confirm this.

The effective lifetimes of the 5533.1 and 5027.3 keV levels were determined from the 225, 258.8, and 1124.8 keV transitions at all average angles. It was not possible to correct for feeding in these states, and the effective lifetimes are given, indicating upper-lifetime limits. Effective lifetimes of $0.97^{+0.24}_{-0.21}$ and $1.09^{+0.38}_{-0.33}$ ps were determined for the 17^+ and 16^+ states, respectively. As can be seen, the states have effective lifetimes which are comparable to those of the 17^+ states in bands 2 and 3.

B. Negative-parity states

Generally, all low-spin ($<16\hbar$) gates in coincidence and below the transition of interest were added together. For cases where interference did not allow this procedure, as for the pairs 1406.4–1425.2, 1089.9–1071.2, and 1124.5–1133.9 keV, fewer gates were added. To increase statistics above the 22^- and 23^- states in bands 5 and 6, gates in coincidence were added starting from lines below the 22^- or 23^- levels, respectively.

For bands 5, 6, 7, and 9 the highest-lying states which could be analyzed in the present work were the 2019 keV (26^-), 1959.6 keV (27^-), 1456 keV (21^-), and 1830 keV (23^-) transitions (levels), respectively. Only effective lifetimes are quoted for these levels, indicating the upper-lifetime limits. The 1287.6 keV line shape was fitted together with the 1258.2 keV line shape. Because of unavoidable interference the line shapes of the 847.3 (band 6) and 1083.1 keV (band 8) transitions could not be analyzed; instead the lifetimes of their parent states were extracted by using the line shapes of the 522.8 and 835.2 keV transitions.

The higher-lying states in band 9 are long lived compared to those in bands 5 and 6. The 19^- state is a very long-lived state as calculated from the 1037.4 keV line shape, ''shadowing'' the lower-lying states. This leads to greater uncertainties for the shorter lifetimes measured for the 1124.5 and 1071.2 keV transitions.

C. Transition strengths

The electric quadrupole transition strengths $B(E2)$ were determined from the accepted lifetimes, transition energies, and branching ratios given in Tables I and II and were used to calculate transition quadrupole moments $|Q_t|$ from the rotational model according to

$$Q_t^2=\frac{16\pi}{5}\langle IK20|I-2K\rangle^{-2}B(E2,I\rightarrow I-2). \qquad (1)$$

A value of $K=6$ was used for all bands (1 to 9). Both quantities $B(E2)$ and the transition quadrupole moments Q_t are given in Table II.

Most magnetic dipole transition strengths $B(M1)$ were calculated using a quadrupole-dipole mixing ratio of $\delta=0$ since $B(M1)$ values are rather insensitive to δ as long as it is small. However, a mixing ratio for the 248.1 keV line was available from Ref. [10] and was used to calculate $B(M1)$ as well as $B(E2)$ for this transition. The magnetic dipole transition strengths for the positive and negative-parity bands are given in Tables III and IV, respectively.

V. DISCUSSION

A. Positive-parity bands

The transition quadrupole moments Q_t determined in the present work are shown graphically in Fig. 9. The Q_t values and hence the quadrupole collectivity in the $\pi g_{9/2}\otimes \nu g_{9/2}$ bands (3 and 4), fall with increasing spin from more than 2.5 e b down to about 1 e b at spin $16\hbar$ and then level off. In a rotational model interpretation, this would correspond to a decrease of quadrupole deformation β_2 from about 0.27 to 0.11 with increasing spin. Although the lifetimes of the lowest states are too long to be measured with the DSAM, an earlier recoil-distance measurement of the mean lifetime of the 8^+ state [9] confirms the higher Q_t values for the lower states.

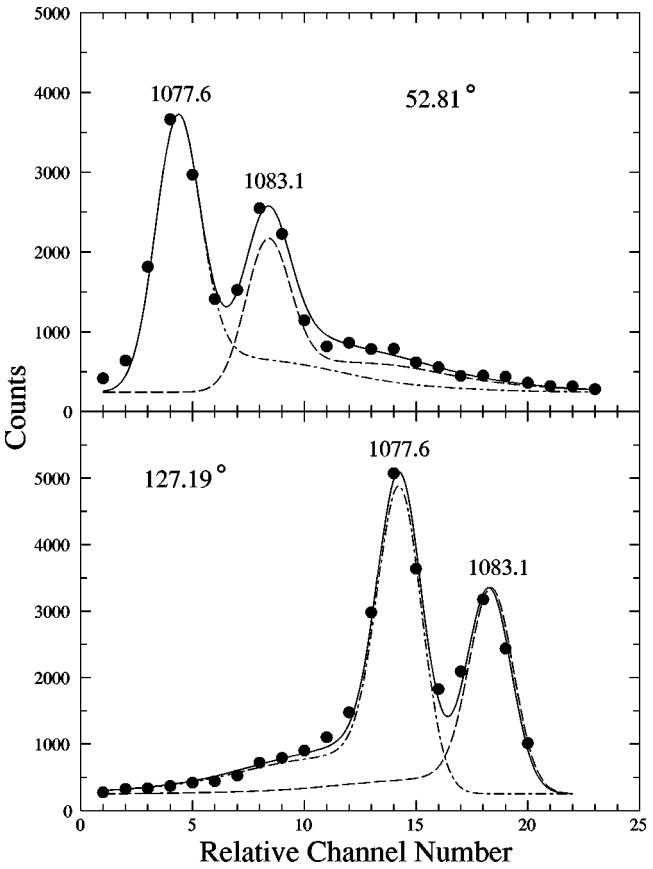

FIG. 8. An illustration of simultaneous fits to the 1077.6 and 1083.1 keV line shapes.

Comparison with a cranked shell model analysis of the level energies and spins shows only a limited correspondence. The kinematic moments of inertia (shown in Fig. 4 of Ref. [8]) are quite flat in the region where Q_t decreases steadily. Then the Q_t value levels out at approximately the point of a small rise in $J^{(1)}$. Although the two graphs agree roughly on the point at which a change occurs, the relation is almost opposite to the conventional wisdom that higher moments of inertia correspond to greater deformations.

Band 2 appears to follow the same trend as bands 3 and 4, although it does not extend as far down in spin. There is certainly no evidence that band 2 is more deformed, as might be expected since it becomes yrast between the 17^+ and 19^+ states and exhibits generally higher moments of inertia. The transition quadrupole moment from the 19^+ state is divided between the 1337.1 keV intraband and the 1113 and 1370.9 keV interband decays, suggesting significant band mixing. However, there appears to be no reduction in the Q_t values for the 1303.4 and 1320.3 keV transitions even though their energies do not increase in the regular way expected for rigid rotors and the 1303.4 keV decay may be more of an interband rather than intraband transition.

The few Q_t values which could be determined in band 1 (not graphed) are smaller than those in the other bands. This is consistent with a smaller deformation for a nonyrast struc-

TABLE II. Energies, branching ratios, electric transition quadrupole strengths, and electric transition quadrupole moments in ^{86}Nb. Energies, spins, and branching ratios were taken from Ref. [8].

E_x (keV)	I_i^π	E_γ (keV)	B (%)	$B(E2)$ [a] (W.u.)	Q_t (e b)
		Band 1			
10429	(23^+)	1827	100.0	>16.1	>1.09
8602	(21^+)	1645	100.0	$6.8^{+3.9}_{-2.3}$	$0.72^{+0.18}_{-0.13}$
6957	(19^+)	1649	60.0	$2.4^{+1.4}_{-0.8}$	$0.44^{+0.11}_{-0.08}$
		1424	40.0	$3.4^{+1.9}_{-1.1}$	$0.52^{+0.13}_{-0.09}$
		Band 2			
13568	(27^+)	2285	100.0	>6.4	>0.67
13509	(27^+)	2226	100.0	>7.4	>0.72
11283	(25^+)	1901	100.0	$14.6^{+9.7}_{-5.5}$	$1.02^{+0.30}_{-0.21}$
9382	23^+	1476	100.0	$16.1^{+5.4}_{-3.2}$	$1.09^{+0.17}_{-0.11}$
7907	21^+	1261	81.5	$14.2^{+6.3}_{-3.6}$	$1.04^{+0.21}_{-0.14}$
6645	19^+	1337	64.9	$6.9^{+2.4}_{-1.5}$	$0.74^{+0.12}_{-0.09}$
		1113	9.8	$2.6^{+0.9}_{-0.6}$	$0.45^{+0.07}_{-0.05}$
		1371	25.3	$2.4^{+0.8}_{-0.5}$	$0.43^{+0.07}_{-0.05}$
5308	17^+	1320	73.5	$11.6^{+3.4}_{-2.3}$	$1.00^{+0.14}_{-0.10}$
3988	15^+	1303	74.8	$23.2^{+9.5}_{-6.1}$	$1.48^{+0.27}_{-0.21}$
		Band 3			
12014	(25^+)	1961	100.0	>20.8	>1.22
10053	(23^+)	1782	100.0	$12.6^{+16.1}_{-4.8}$	$0.96^{+0.49}_{-0.21}$
8271	(21^+)	1548	100.0	$22.6^{+14.4}_{-8.1}$	$1.31^{+0.37}_{-0.26}$
6723	19^+	1448	64.5	$13.6^{+12.6}_{-5.1}$	$1.04^{+0.40}_{-0.22}$
		1414	27.8	$6.6^{+6.1}_{-2.4}$	$0.73^{+0.28}_{-0.15}$
5274	17^+	1371	60.8	$10.3^{+2.6}_{-2.0}$	$0.94^{+0.11}_{-0.10}$
		1287	29.1	$6.8^{+1.7}_{-1.3}$	$0.76^{+0.09}_{-0.08}$
3903	15^+	1218	82.7	$22.7^{+3.1}_{-3.2}$	$1.47^{+0.10}_{-0.11}$
2684	13^+	1083	66.3	$31.6^{+8.6}_{-6.8}$	$1.87^{+0.24}_{-0.21}$
1601	11^+	877	36.0	$51.4^{+16.7}_{-12.0}$	$2.76^{+0.42}_{-0.34}$
		Band 4			
6362	(18^+)	1521	100.0	>10.3	>0.92
4841	16^+	1373	100.0	$9.9^{+4.7}_{-2.6}$	$0.94^{+0.20}_{-0.13}$
3468	14^+	1256	85.8	$19.8^{+5.6}_{-4.3}$	$1.42^{+0.19}_{-0.16}$
2212	12^+	1078	88.1	$32.8^{+5.1}_{-4.6}$	$2.02^{+0.15}_{-0.15}$
275	8^+	275	56.1	$10.7^{+3.3}_{-2.0}$	$2.53^{+0.36}_{-0.25}$
		Band 5			
12885	(26^-)	2019	100.0	>33.7	>1.54
10866	24^-	1802	100.0	$31.8^{+15.9}_{-10.6}$	$1.51^{+0.34}_{-0.28}$
9064	22^-	1604	100.0	$42.6^{+14.2}_{-8.5}$	$1.78^{+0.28}_{-0.19}$
7460	20^-	1425	100.0	$32.4^{+11.6}_{-8.7}$	$1.59^{+0.26}_{-0.23}$
6035	18^-	1258	100.0	$60.4^{+11.3}_{-10.5}$	$2.23^{+0.20}_{-0.20}$
4777	16^-	1090	84.9	$40.8^{+5.7}_{-5.7}$	$1.91^{+0.13}_{-0.14}$
3687	14^-	908	73.6	$39.7^{+5.4}_{-5.1}$	$2.00^{+0.13}_{-0.13}$
		Band 6			
13416	(27^-)	1960	100.0	>22.7	>1.26
11457	25^-	1728	100.0	$19.6^{+6.5}_{-4.9}$	$1.18^{+0.18}_{-0.16}$
9729	23^-	1514	100.0	$56.8^{+18.9}_{-15.5}$	$2.04^{+0.32}_{-0.30}$
8214	21^-	1406	100.0	$36.5^{+7.3}_{-6.6}$	$1.67^{+0.16}_{-0.16}$
6808	19^-	1303	100.0	$38.5^{+7.3}_{-6.4}$	$1.75^{+0.16}_{-0.15}$
5504	17^-	1134	50.4	$21.2^{+5.1}_{-4.1}$	$1.34^{+0.15}_{-0.14}$
		1187	42.9	$14.3^{+3.5}_{-2.7}$	$1.11^{+0.13}_{-0.11}$
4318	15^-	1016	64.9	$31.5^{+7.3}_{-5.9}$	$v1.72^{+0.19}_{-0.17}$
3302	13^-	847	25.6	$32.6^{+5.2}_{-4.3}$	$1.90^{+0.15}_{-0.13}$
		Band 7			
8428	(21^-)	1456	100.0	>24.0	>1.35
6972	(19^-)	1367	100.0	$21.1^{+5.1}_{-3.8}$	$1.30^{+0.15}_{-0.12}$
5605	17^-	1288	100.0	$48.7^{+155.9}_{-22.5}$	$2.04^{+2.14}_{-0.54}$
		Band 8			
5153	16^-	1083	42.7	$34.5^{+80.7}_{-16.4}$	$1.76^{+1.45}_{-0.48}$
		Band 9			
9649	(23^-)	1830	100.0	>5.3	>0.63
7819	21^-	1340	100.0	$7.3^{+1.8}_{-1.4}$	$0.75^{+0.11}_{-0.09}$
6479	19^-	1037	100.0	$16.6^{+3.3}_{-2.9}$	$1.15^{+0.11}_{-0.11}$
5442	17^-	1071	43.0	$52.6^{+39.4}_{-19.1}$	$2.12^{+0.68}_{-0.43}$
		1125	31.2	$29.9^{+22.4}_{-10.9}$	$1.60^{+0.52}_{-0.32}$
4371	15^-	993	81.8	$34.1^{+4.7}_{-4.3}$	$1.79^{+0.12}_{-0.12}$
3377	13^-	779	34.8	$46.8^{+33.2}_{-15.8}$	$2.28^{+0.70}_{-0.42}$
		923	39.3	$22.6^{+16.0}_{-7.6}$	$1.58^{+0.49}_{-0.30}$

[a] 1 W.u. $=22.55\ e^2\ \mathrm{fm}^4$.

TABLE III. Energies, branching ratios, and magnetic dipole transition strengths in the positive-parity bands.

E_x (keV)	I_i^π	E_γ (keV)	B (%)	$B(M1)$[a] (μ_N^2)
7907	21^+	241	18.5	$1.162^{+0.516}_{-0.294}$
6723	19^+	361	7.7	$0.347^{+0.322}_{-0.249}$
5533	(17^+)	505	51.1	>0.233
		259	27.7	>0.940
		225	21.3	>1.099
5308	17^+	467	26.5	$0.260^{+0.077}_{-0.051}$
5274	17^+	434	10.1	$0.160^{+0.041}_{-0.032}$
5027	(16^+)	1125	100.0	>0.037
3988	15^+	519	25.2	$0.331^{+0.135}_{-0.087}$
3903	15^+	434	17.3	$0.246^{+0.034}_{-0.035}$
3468	14^+	785	14.2	$0.034^{+0.009}_{-0.007}$
2684	13^+	472	33.7	$0.358^{+0.098}_{-0.077}$
2212	12^+	610	11.9	$0.045^{+0.007}_{-0.006}$
1601	11^+	467	64.0	$0.732^{+0.237}_{-0.172}$
275	8^+	248	43.9	$0.135^{+0.041}_{-0.026}$ [b]

[a]For reference, 1 W.u. $=1.79\,\mu_N^2$.
[b]$B(M1)$ multiplied by 100.

ture. Again, the decay strength out of the 19^+ state in this band is divided into two $\Delta I=2$ branches.

The $B(M1)$ strengths between signature partner bands 3 and 4, graphed in Fig. 10, confirm the oscillations suggested by the $B(M1)/B(E2)$ ratios in Fig. 7 of Ref. [8]. Together, the two graphs show an unbroken alternating pattern from the 8^+ to the 19^+ state with no sign of the phase reversal seen in the energy differences around spin $10\hbar$. This difference between the signature splitting patterns of the energies and $M1$ strengths has been seen consistently in the $\pi g_{9/2}\otimes \nu g_{9/2}$ bands [1], but still awaits theoretical understanding.

It is interesting that some of the strongest $M1$ transitions observed ($1\,\mu_N^2$) connect bands 2 and 3 with the ''extra'' states at 7666 and 5533.1 keV. On the other hand, no $E2$ transitions were observed connecting these or the 5027.3 keV state with any of the bands. Limits for the unobserved branches suggest $B(E2)$ strengths less than 0.5 W.u. for possible decays such as $(17^+)\rightarrow 15^+$ or $(16^+)\rightarrow 14^+$. Strong $M1$ and weak $E2$ transitions support the picture of single-particle or aligned character for these ''extra'' states.

B. Negative-parity bands

The grouping of decay sequences into bands is not always clear if significant mixing occurs. The behavior of the Q_t values determined in the present work suggested a different arrangement than that of Ref. [8]. Basically the portions of bands 6 and 9 from the 17^- states upward have been interchanged. In this picture the 1071.2 and 1186.5 keV transitions are viewed as in-band, rather than the 1124.5 and 1133.9 keV decays, which were considered in-band transitions in Ref. [8]. Of course, the reality is that there is considerable mixing between the 15^- and 17^- states in the two bands no matter how they are grouped.

TABLE IV. Energies, branching ratios, and magnetic dipole transition strengths in the negative-parity bands.

E_x (keV)	I_i^π	E_γ (keV)	B (%)	$B(M1)$[a] (μ_N^2)
5504	17^-	727	6.8	$0.022^{+0.005}_{-0.004}$
5442	17^-	289	13.9	$1.570^{+1.177}_{-0.571}$
		665	12.0	$0.111^{+0.083}_{-0.040}$
5153	16^-	783	27.0	$0.107^{+0.250}_{-0.051}$
		835	30.3	$0.099^{+0.231}_{-0.047}$
4777	16^-	459	15.1	$0.182^{+0.025}_{-0.026}$
4371	15^-	300	18.2	$0.426^{+0.259}_{-0.054}$
4318	15^-	631	35.1	$0.116^{+0.027}_{-0.022}$
4070	14^-	768	100.0	$0.194^{+0.177}_{-0.072}$
3687	14^-	385	26.4	$0.242^{+0.033}_{-0.031}$
3377	13^-	598	25.9	$0.074^{+0.059}_{-0.025}$
3302	13^-	523	74.4	$0.457^{+0.073}_{-0.061}$

[a]For reference, 1 W.u. $=1.79\,\mu_N^2$.

Because of the rearrangement in suggested band structure, the kinematic moments of inertia $J^{(1)}$ for the negative-parity bands have been recalculated and are displayed in Fig. 11. Now the $J^{(1)}$ values in signature-partner bands 5 and 6 are rather similar throughout the entire frequency range. The weak broad peak at $\hbar\omega\approx$ 0.75 MeV seen only in odd-spin band 6 may result from mixing with bands 7 or 9.

Under the present band interpretation, the Q_t values in bands 5 and 6 are also quite similar throughout the entire spin range except for the dip at the most strongly mixed 17^- state. In contrast, the transition quadrupole moments in band 9 above the 17^- state fall significantly lower than those in bands 5 and 6 and are comparable only to those in band 1. This again represents a reversal of the commonly held expectation that larger deformations are associated with greater moments of inertia. Band 9 is yrast in the 17^- to 23^- spin range and has larger moments of inertia but its Q_t values are significantly lower.

The transition quadrupole moments in bands 5 and 6 are somewhat intermediate between the range of values seen in positive-parity bands 3 and 4. The overall trend is perhaps a slow decrease with increasing spin. In a rotational model interpretation, this would correspond to quadrupole deformations β_2 ranging from about 0.22 down to about 0.15.

It would have been very interesting to explore the collectivity of the states below 13^- because an extrapolation of

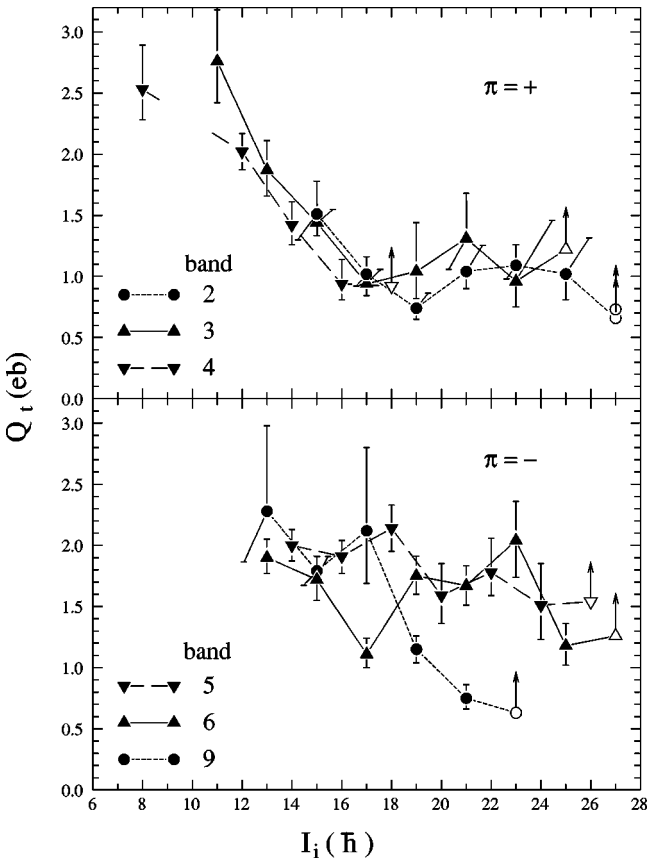

FIG. 9. The electric quadrupole moments $|Q_t|$ vs the initial spin I_i for the positive-parity bands 2, 3, and 4 (top) and for the negative-parity bands 5, 6, and 9 (bottom). Open symbols correspond to lower limit values. The lifetime of the 10^+ level in band 4 is not known, and that for the 8^+ level has been taken from [9].

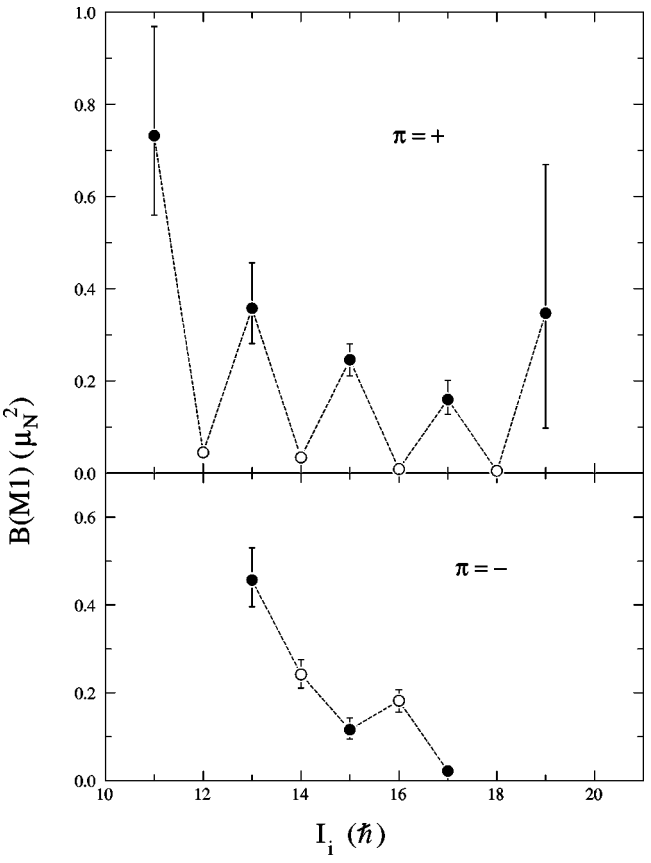

FIG. 10. The magnetic dipole transition strengths $B(M1)$ vs the initial spin I_i for the yrast positive-parity band and negative-parity band. States in which I_i has even (odd) spin are shown with open (filled) symbols.

Fig. 9 would suggest increasing collectivity with decreasing spin, but the almost constant transition energies between the lower-spin states argue for lower collectivity. Unfortunately their lifetimes could not be measured using the DSAM because their line shapes exhibit almost no Doppler shifting.

The $B(M1)$ values between bands 5 and 6 generally decrease with increasing spin. There is no evidence for alternations.

C. Hartree-Fock-Bogoliubov cranking calculations

Hartree-Fock-Bogoliubov cranking calculations [14] were performed for configurations in ^{86}Nb using a Woods-Saxon potential and a short-range monopole pairing force. Total Routhian surface (TRS) plots in the (β_2, γ) plane were generated from these calculations. Figure 12 shows four TRS plots at two different frequencies. At each grid point, the Routhian was minimized with respect to the hexadecapole deformation β_4. The quasiparticle labeling scheme was taken from Ref. [15] with lower (upper) case letters representing proton (neutron) configurations. The label ''aA'' stands for the lowest proton and neutron configuration yielding overall positive parity and signature $\alpha=1$ (odd spin), while label ''aE'' is the lowest two quasiparticle configuration with overall negative parity and even spin.

The deepest minima in most of the total Routhian surfaces calculated for ^{86}Nb correspond to spherical shapes or noncollective rotation. They would imply [16–19] Q_t values of zero, in contrast to the observed range of 0.5 to 2.5 e b. A shallow, triaxial to oblate minimum with $\beta_2 \approx 0.15$ can be seen in all four TRS plots in Fig. 12. It leads to Q_t values in

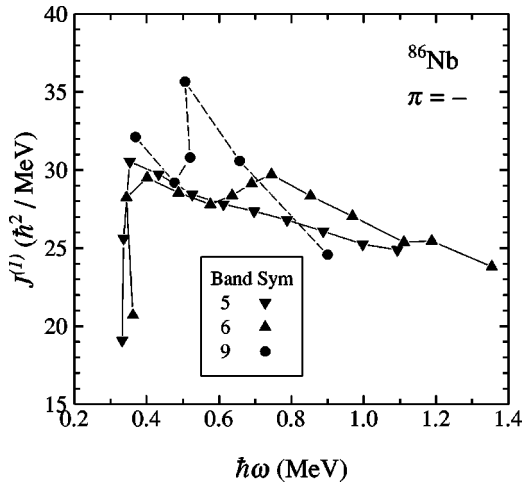

FIG. 11. Kinematic moments of inertia $J^{(1)}$ as a function of rotational frequency ω for the negative-parity bands of ^{86}Nb.

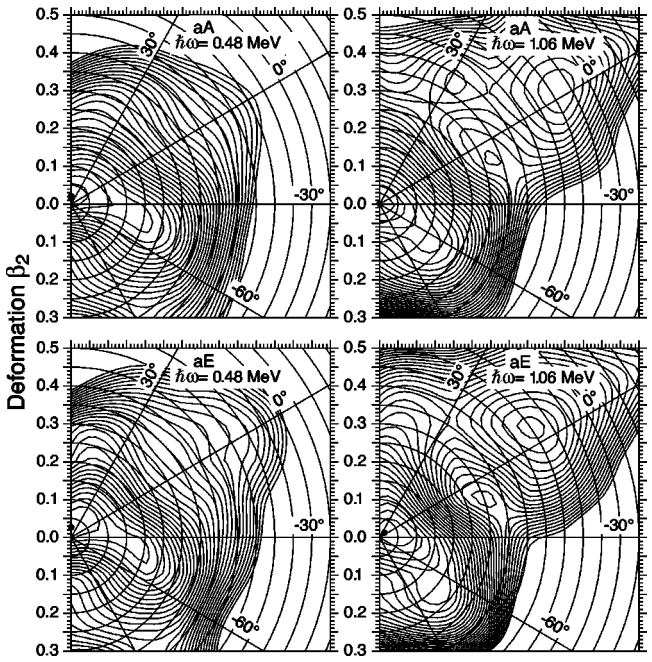

FIG. 12. Calculated total Routhian surfaces for ^{86}Nb in the (β_2,γ) polar coordinate plane for two rotational frequencies and two different configurations. The aA [aE] configuration corresponds to $(\pi,\alpha)=(+,1)$ $[(-,0)]$. The spacing between contour lines is 250 keV.

the range of 1 to 2 e b and is the best candidate to match the experimentally observed structures.

More minima appear in the TRS at higher rotational frequencies, but they are too deformed to correspond to the observed states. For example, the prolate minimum at $\beta_2 \approx 0.5$ appears rather consistently at higher frequencies, but the Q_t values associated with this ''superdeformed'' shape (5 to 7 e b) are a factor of 2 to 4 larger than those measured in the present work. The near prolate shapes with $\beta_2 \approx 0.3$ imply Q_t values of about 3.5 e b and do not appear at lower frequencies where the highest transition quadrupole moments were observed experimentally.

Therefore the measured lifetimes show that the only structures in the TRS which can correspond to the observed bands are those with $0.1 \leqslant \beta_2 \leqslant 0.2$ and $-70° \leqslant \gamma \leqslant -30°$. It is difficult to make a more detailed comparison between the predicted and observed Q_t values because these triaxial to oblate minima are so shallow and β soft. Although there are indications of minima in the region at most frequencies, it is often not possible to determine the location of the minima with enough accuracy or confidence to decide whether the variation with spin agrees or disagrees with the patterns seen experimentally.

VI. SUMMARY

The fusion-evaporation reaction ^{58}Ni(^{32}S,3pn) with a beam energy of 135 MeV was used to populate high-spin states in ^{86}Nb. The full Gammasphere array and the Microball were used to detect multi-γ coincidences with evaporated charged particles. Since a thick backing material was used, lifetime measurements of 51 states in ^{86}Nb were performed at four detector angles using the Doppler-shift attenuation method. Triple γ coincidences and charged particle gates were used to extract clean line shapes. Side-feeding times were measured directly for some states by comparing line shapes fitted from spectra gated above and below. Transition quadrupole moments Q_t calculated from the lifetimes in the yrast positive-parity bands decrease from 2.7 e b at low spins to 1.0 e b at spin $17\hbar$ and then remain relatively constant. This would correspond to quadrupole deformations β_2 decreasing from 0.27 to 0.11 in an axial rotational model. The magnetic dipole transition strengths $B(M1)$ between the two signatures show strong oscillations with no sign of the phase reversal seen in the energy signature splittings. The Q_t values in band 2 are quite similar to those in bands 3 and 4 even though the energies of the lower states do not increase as expected for a rigid rotor and the higher states become yrast.

The transition quadrupole moments in negative-parity bands 5 and 6 average about 1.7 e b ($\beta_2 \sim 0.19$) with perhaps a gentle decrease with increasing spin. Those in band 9 are comparable at low spins, but decrease considerably above spin $17\hbar$. A number of interband transitions suggest considerable mixing between bands 6 and 9, especially for the 17^- states. Based on the similarities and differences among the Q_t values, the upper portions of bands 6 and 9 have been interchanged.

Hartree-Fock-Bogoliubov cranking calculations were performed to compare with the experimental results. Somewhat shallow minima were found in the total Routhian surfaces at triaxial to oblate shapes with $0.1 \leqslant \beta_2 \leqslant 0.2$ which appear to correspond to the observed positive- and negative-parity bands. The measured Q_t values clearly rule out both the spherical and highly-deformed minima in the TRS. Although the moderately deformed triaxial to oblate minima appear consistently over a wide range of rotational frequencies and imply Q_t values in the range observed experimentally, it is difficult to locate the positions of these shallow minima accurately enough to test whether they can reproduce the observed variations with spin.

ACKNOWLEDGMENTS

This work was supported in part by the National Science Foundation under Grant No. PHY-9523974 (FSU) and in part by the Department of Energy under Contract Nos. DE-AC05-76OR00033 (UNISOR), DE-AC05-96OR22464 (ORNL), DE-FG05-88ER40406 (WU), and DE-AC03-76SF00098 (LBNL). F.C. acknowledges support from Colciencias (Bogotá), Contract No. 222-96. We are grateful to W. Nazarewicz for providing the results of his Hartree-Fock-Bogoliubov calculations.

[1] S.L. Tabor, Heavy Ion Phys. **2**, 239 (1995).
[2] E. Landulfo, D.F. Winchell, J.X. Saladin, F. Cristancho, D.E. Archer, J. Döring, G.D. Johns, M.A. Riley, S.L. Tabor, V.A. Wood, S. Salém-Vasconcelos, and O. Dietzsch, Phys. Rev. C **54**, 626 (1996).
[3] J. Döring, D. Pantelica, A. Petrovici, B.R.S. Babu, J.H. Hamilton, J. Kormicki, Q.H. Lu, A.V. Ramayya, O.J. Tekyi-Mensah, and S.L. Tabor, Phys. Rev. C **57**, 97 (1998).
[4] R.A. Kaye, L.A. Riley, G.Z. Solomon, S.L. Tabor, and P. Semmes, Phys. Rev. C **58**, 3228 (1998).
[5] J. Döring, D. Ulrich, G.D. Johns, M.A. Riley, and S.L. Tabor, Phys. Rev. C **59**, 71 (1999).
[6] M.A. Cardona, G. García Bermúdez, R.A. Kaye, G.Z. Solomon, and S.L. Tabor, Phys. Rev. C **61**, 044316 (2000).
[7] C.J. Gross, K.P. Lieb, D. Rudolph, M.A. Bentley, W. Gelletly, H.G. Price, J. Simpson, D.J. Blumenthal, P.J. Ennis, C.J. Lister, Ch. Winter, J.L. Durell, B.J. Varley, Ö. Skeppstedt, and S. Rastikerdar, Nucl. Phys. **A535**, 203 (1991).
[8] S.L. Tabor, J. Döring, G.D. Johns, R.A. Kaye, G.N. Sylvan, C.J. Gross, Y.A. Akovali, C. Baktash, D.W. Stracener, P.F. Hua, M. Korolija, D.R. LaFosse, D.G. Sarantites, F.E. Durham, I.Y. Lee, A.O. Macchiavelli, W. Rathbun, and A. Vander Molen, Phys. Rev. C **56**, 142 (1997).
[9] R.A. Kaye, J.B. Adams, A. Hale, C. Smith, G.Z. Solomon, S.L. Tabor, G. García-Bermúdez, M.A. Cardona, A. Filevich, and L. Szybisz, Phys. Rev. C **57**, 2189 (1998).
[10] M.W. Cooper, D.J. Hartley, R.A. Kaye, K.W. Kemper, M.A. Riley, C. Smith, G.Z. Solomon, D.A. Soltysik, and S.L. Tabor, Phys. Rev. C **59**, 2268 (1999).
[11] I.Y. Lee, Nucl. Phys. **A520**, 641c (1990).
[12] D.G. Sarantites, P.-F. Hua, M. Devlin, L.G. Sobotka, J. Elson, J.T. Hood, D.R. LaFosse, J.E. Sarantites, and M.R. Maier, Nucl. Instrum. Methods Phys. Res. A **381**, 418 (1996).
[13] E.F. Moore, P.D. Cottle, C.J. Gross, D.M. Headly, U.J. Hüttmeier, S.L. Tabor, and W. Nazarewicz, Phys. Rev. C **38**, 696 (1988).
[14] W. Nazarewicz, J. Dudek, R. Bengtsson, T. Bengtsson, and I. Ragnarsson, Nucl. Phys. **A435**, 397 (1985).
[15] R. Wyss, F. Lidén, J. Nyberg, A. Johnson, D.J.G. Love, A.H. Nelson, D.W. Banes, J. Simpson, A. Kirwan, and R. Bengtsson, Nucl. Phys. **A503**, 244 (1989).
[16] P. Ring, A. Hayashi, K. Hara, H. Emling, and E. Grosse, Phys. Lett. **110B**, 423 (1982).
[17] I. Hamamoto and B.R. Mottelson, Phys. Lett. **132B**, 7 (1983).
[18] W. Nazarewicz, M.A. Riley, and J.D. Garrett, Nucl. Phys. **A512**, 61 (1990).
[19] J. Dudek, W. Nazarewicz, and P. Olanders, Nucl. Phys. **A420**, 285 (1984).